Mine Water Environ (2017) 36:299–309
DOI 10.1007/s10230-016-0399-z

TECHNICAL ARTICLE

Quantifying Iron Concentration in Local and Synthetic Acid Mine Drainage: A New Technique Using Handheld Field Spectrometers

Gwendolyn E. Davies[1] · Wendy M. Calvin[1]

Received: 17 September 2015 / Accepted: 29 March 2016 / Published online: 18 April 2016

Abstract Pit lakes present a concern for public safety and environmental quality. With continuing advancement of imaging satellites, remote sensing spectroscopy may provide a useful tool for monitoring pit water quality across vast mining districts. Visible to shortwave infrared remote sensing has been widely used to monitor acid mine drainage (AMD) mineralogy at mine sites. However, few studies have examined the spectral signatures of mine-affected waters and open pit water bodies from a remote platform. The motivation for this study was to identify the spectral characteristics of AMD in a controlled laboratory setting in order to better interpret mine water bodies in remote sensing imagery. The spectral response of synthetic and local AMD were measured using a field spectrometer. Solutions with increasing Fe^{3+} and Fe^{2+} concentrations were mixed to mimic the chemical properties of local AMD. Synthetic solutions with known Fe concentrations were compared with local AMD for quantitative assessment. The spectral signatures of Fe^{3+} dominated waters possessed distinct characteristics that may be used for diagnostic identification. Specifically, the region between 0.35 and 0.625 μm was used to approximately quantify Fe^{3+} concentrations. Subtle changes in Fe concentrations in local AMD were identified using a field spectrometer alone. These findings suggest that subtle changes in open pit water quality may also be qualitatively and quantitatively measured by remote sensing spectroscopy.

Keywords Aqueous ferric iron · Environmental monitoring · Mine waste · Spectroscopy

Introduction

One of the major environmental issues facing the global mining industry is the water quality of open pit lakes (Castendyk and Eary 2009). By 2025, almost 50 open pit mines that intercept the groundwater table will be completed in the USA (Vandersluis et al. 1995). In the state of Nevada alone, 35 mines will have a lake in their open pit after dewatering ceases (Shevenell 2000). Improved technologies for monitoring these potentially environmentally hazardous features are needed. Open pits range in size from relatively small pits about 100 m in diameter, to enormous open cut operations such as the Bingham Canyon copper mine in Utah, which measures 4 km wide and 1.2 km deep (Castendyk and Eary 2009; McCullough et al. 2011). These large footprints are observable from imaging satellites (Peichang et al. 2004; Sanliyuksel et al. 2014). With the continuing advancement of imaging satellites, remote sensing may provide a useful monitoring tool for snapshots of pit water quality across large mining districts. This paper will explore the potential use of visible to short wave infrared (VSWIR) spectroscopy for water quality analysis in pit lakes. The results of this paper are intended to lay a foundation for subsequent application to remote sensing spectroscopy. The objectives are to: (1) identify the unique spectral response of acid mine discharge (AMD) from a local source in a laboratory setting, (2) identify the spectral response of simplified synthetic mine water in a laboratory

Electronic supplementary material The online version of this article (doi:10.1007/s10230-016-0399-z) contains supplementary material, which is available to authorized users.

✉ Gwendolyn E. Davies
gwen.davies.11@gmail.com

[1] Department of Geologic Sciences and Engineering, University of Nevada, Reno, Mailstop 172, 1664 N Virginia St, Reno, NV 89503, USA

setting, and (3) compare the local and synthetic datasets in order to make a qualitative and quantitative assessment on the diagnostic spectral features of AMD.

Background

The oxidation of sulfide minerals releases hydrogen ions into mine water, in addition to liberating metals and sulfate. AMD is associated with the release of sulfate, metals (Fe, Cu, Pb, Zn, Cd, Co, Cr, Ni, Hg), metalloids (As, Sb, Se, Te), and other elements, such as Si, Ca, Na, K, Mg, and Ba (Lottermoser 2003). These waters are characterized by exceptionally high sulfate (>1000 mg/L), high iron and aluminum (>100 mg/L), and elevated copper, chromium, nickel, lead, and zinc concentrations (>10 mg/L; Lottermoser 2003). Many pit lakes from former gold, metal-sulfide, or coal mines contain significant concentrations of metals and/or metalloids, acidic pH, high total dissolved solids (TDS), and elevated turbidity (Gammons et al. 2009).

The iron cation strongly affects the 0.4–1.1 μm portion of the VSWIR region, producing diagnostic absorption minima that may be used for mineral identification (Burns 1993; Hunt and Ashley 1979). Iron was chosen for the focus of this study because of its spectral robustness and high concentrations in pit lakes. Poor water quality in open pit lakes or AMD discharge is commonly recognized by the water's intense red color associated with these high iron concentrations. One of the most extreme examples of this is the Berkeley Pit Lake in southwestern Montana. Approximately 39 billion gallons of red water are contained in the lake, with a surface water composition of pH 2.75 and 484 mg/L Fe (Duaime and Tucci 2009).

This study examined the AMD at the Leviathan Mine Superfund site, located in the Monitor Pass mining district in Alpine County, California (Fig. 1). The Leviathan Mine is a high sulfidation epithermal replacement deposit (Evans 1977). Approximately 5.08×10^8 kg of elemental sulfur were extracted from Leviathan during open pit mining from 1952 to 1962 (Evans 1977). The primary source of AMD emanates from discharging groundwater from a remnant tunnel and adit structure. Currently, AMD is collected in a series of evaporation ponds and treated at an on-site facility (California Regional Water Quality Control Board 2015). Fresh AMD from the adit/tunnel is piped to the south end of Pond 1 (Fig. 1). From there, water is distributed between Pond 1, Pond 2 South, and Pond 2 North, which are interconnected and are at the same elevation. Excess water may be released down to Pond 3 for additional storage if necessary. Water is stored in the ponds throughout the winter and spring before being pumped into the treatment facility in mid-summer. As the AMD oxidizes and accumulates in the ponds, it becomes strikingly red in color (Fig. 1 and supplemental Fig. 1a, b). During the time of this study, Pond 3 was not used for AMD storage. Only meteoric water was present in Pond 3 in the spring. In 2014, AMD was treated between September 8 and 12.

Methods

Local AMD Waters

Reconnaissance data was collected at Leviathan Mine on 05/22/14. Water samples were taken near the inlet pipe in Pond 1, on the east shore of Pond 2 South, and on the south edge of Pond 3. Samples were collected in HDPE bottles supplied by SEM, Inc. (Reno, NV), stored on ice, and delivered to the SEM, Inc. laboratory for basic water chemistry analysis including major anions/cations, trace elements, ferric/ferrous iron, TDS, pH, redox potential, and turbidity (Al, B, Ca, Fe, Mg, K, SiO_2, and Na by ICP-OES; Sb, As, Ba, Be, Cd, Cr, Co, Cu, Pb, Mn, Ni, Se, Ag, Tl, and Zn by ICP-MS; Cl, F, NO_3, and SO_4 by Ion Chromatography; P by Colorimeter; Hg by AA Cold Vapor).

Water samples for laboratory spectral analysis were taken on 08/08/14 and 10/09/14. At each visit, water samples were collected in HDPE Nalgene containers from all ponds with standing water, stored on ice, and analyzed within 48 h. Samples were taken directly from the inlet pipe in Pond 1, on the north shore of Pond 1, and on the east shore of Pond 2 North (Pond 2 North was safer to access for sampling than Pond 2 South on 08/08/14 and 10/09/14). On all sampling occasions, field pH was measured with a Double Junction Waterproof pHTestr® 20, calibrated using pH 4 and 7 buffer solutions.

On 08/08/14, Pond 3 had dried up while Pond 1, Pond 2 North, and Pond 2 South were slightly lower than their previous levels on 05/22/14. On 10/09/14, water samples were collected from Pond 1 at the inlet and Pond 2 North, and analyzed for ferric/ferrous iron, TDS, pH, redox potential, and turbidity by SEM, Inc. Iron was identified as the principal spectral absorption component in local AMD; therefore, a full set of metal analysis was deemed unnecessary. During the 10/09/14 sampling, Pond 2 South was essentially dry, while Pond 2 North still contained several inches of water. Pond 1 was notably lower than its level during the previous two samplings.

Each water sample was filtered through a 0.45 μm cellulose nitrate filter membrane to separate fine particulates. Two spectral measurements were made on each water sample; filtered and unfiltered solutions. Spectral measurements were taken using a FieldSpec ASD spectrometer, which collects spectral reflectance from 0.35 to 2.5 μm in 2151 bands at 1 nm sampling interval. 100 mL of each

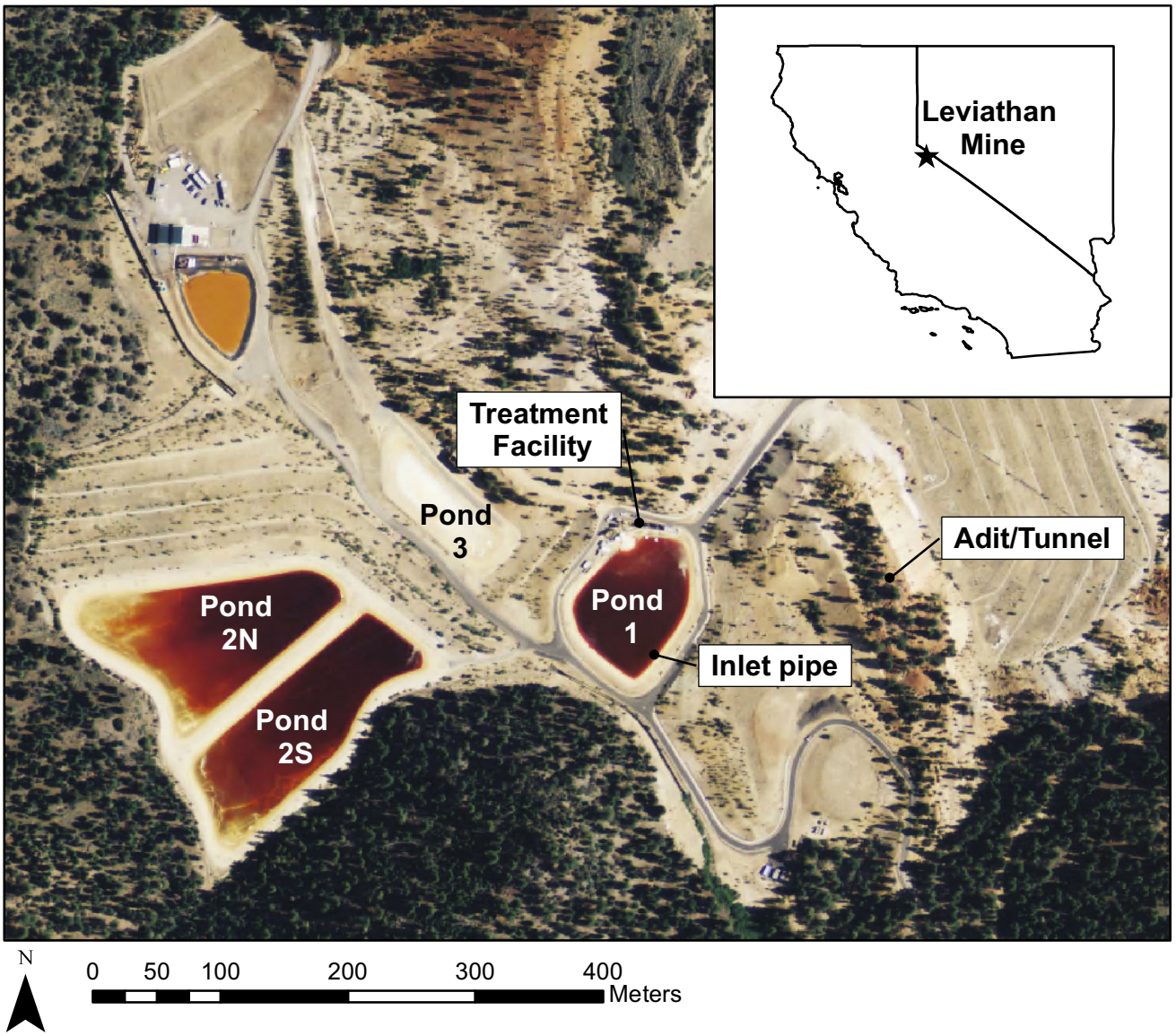

Fig. 1 Leviathan Mine is located in Alpine County, California, 10 miles east of Markleeville and 2 miles north of the Monitor Pass Highway (Sections 15 and 22, Township 10N, Range 21E)

solution was placed in a 150 mL Pyrex beaker, resting on top of a halon plate (a white reference that contains no spectral features). Spectral measurements were made in a dark room using the ASD's contact probe with a halogen light source. The probe was placed on top of the beaker just above the water level. The ASD collection program was set to average 60 individual spectra in each measurement to minimize noise. The resulting spectral response was a combination of water surface reflectance, volume reflectance within the beaker, and bottom reflectance from the halon plate (Fig. 2).

The filtrates were stored in covered plastic petri dishes and allowed to dry at room temperature. Spectral measurements were made directly on the filter paper using the contact probe with halogen light source. A blank filter was also measured, making it possible to distinguish the properties exclusive to the filter membranes.

For comparison to natural water bodies, an additional water sample was taken on 08/07/14 from the East Fork of the Carson River, about 6 miles west of Leviathan Mine on CA highway 89. It had rained several days prior to this sampling, resulting in a turbid sample.

Synthetic AMD Solutions

Synthetic ferric iron solutions were prepared by dissolving reagent grade iron (III) sulfate hydrate ($Fe_2(SO_4)_3$, Sigma Aldrich) into deionized (DI) water. Fifteen solutions of

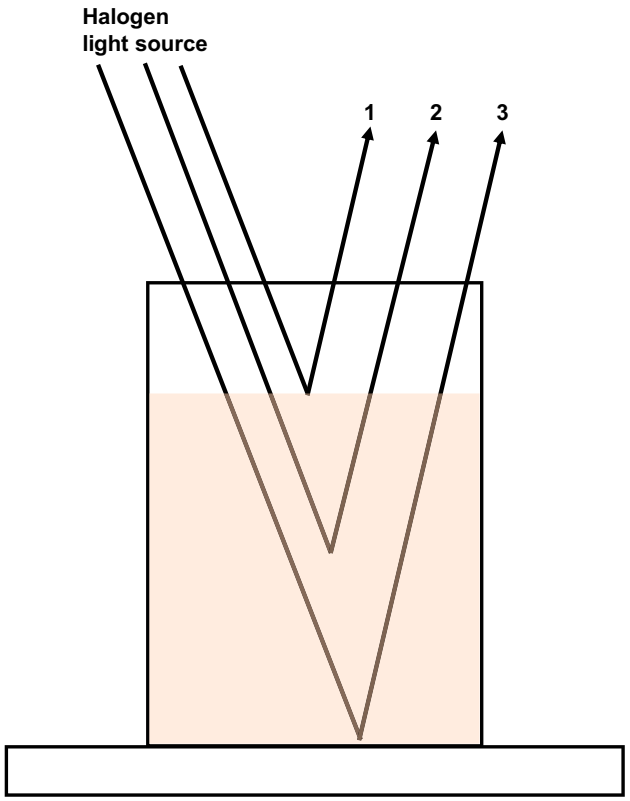

Fig. 2 Schematic of beaker solution and reflected light path. Halogen light source was from the ASD spectrometer probe attachment. *1* Spectral reflectance from water surface. *2* Volumetric scattering and reflectance. *3* Bottom reflectance from halon plate. The total reflectance signature read by the ASD is a combination of all three light paths. Not drawn to scale

increasing ferric iron concentration were produced to mimic the concentrations typically observed in AMD (25–5000 mg/L Fe^{3+}). 100 mL of DI water was mixed with reagent in a 150 mL Pyrex beaker with glass stirring rod. The solutions were stirred until no $Fe_2(SO_4)_3$ particulates were visibly suspended. The pH of the solutions was monitored throughout the experiment. When $Fe_2(SO_4)_3$ dissolves in water, protons are produced by the hydrolysis of $Fe_2(SO_4)_3$ and the pH is reduced. The resulting solution pHs were comparable to that of Leviathans' waters (pH 3.06–1.73). Spectral measurements were made immediately after mixing using the same technique stated above. The solutions varied visually from a faint brown color in the 25 mg/L Fe^{3+} solution to a dark reddish brown color in the 5000 mg/L Fe^{3+} solution.

Using the same techniques, a second batch of synthetic solutions were made with ferrous iron. Reagent grade iron (II) sulfate heptahydrate ($FeSO_4{\cdot}7H_2O$, Sigma Aldrich) was dissolved in DI water. Eight different solutions of increasing Fe^{2+} concentration were produced to mimic the concentrations typically observed in AMD (25–1000 mg/L Fe^{2+}). The solutions were again mixed until no undissolved particles were visually suspended. The solution pHs were acidified to approximately 2.7 using dilute sulfuric acid (H_2SO_4). All solutions were colorless.

The spectral data was analyzed using the continuum removed (CR) method (Clark and Roush 1984). The continuum of a spectrum is a convex hull fit over the top of the spectrum using straight-line segments that connect spectral maximums (Kruse et al. 1993). The continuum is always convex and does not cross through the original spectrum (supplemental Fig. 2). Dividing the spectrum by its continuum results in a CR spectrum containing normalized reflectance values from 0.0 to 1.0. Absorption features, which occur superimposed on a background slope in the original data, are transformed into features with a uniform, flat background of 1.0 in the CR spectrum. This allows the strength (band depth) of each absorption feature to be quantitatively analyzed with respect to a consistent reference level.

Results

Local AMD Waters

Water Chemistry

Water chemistry analyses from 05/22/14 and 10/09/14 are summarized in Tables 1 and 2, respectively. The chemistry of Pond 1 inlet and Pond 2 South on 05/22/14 were similar. The pH was very acidic (2.6–2.8) and the waters contained substantial concentrations of metals and sulfate. Most ion concentrations were comparable between the two. Pond 1 inlet had a slightly lower redox potential than Pond 2 South; 663 versus 721 mV, respectively. As a result, iron speciation was different between the two samples. Pond 1 inlet contained mostly Fe^{2+}, while Pond 2 South contained mostly Fe^{3+}; Fe^{3+}/Fe^{2+} ratios for Pond 1 inlet and Pond 2 South were 0.179 and 8.75, respectively. The chemistry of Pond 3 was considerably different from the other ponds. Although still very poor in quality, Pond 3 had a higher pH and did not contain exceptionally high Fe concentrations. Pond 3 had notably higher concentrations of Al, Co, Mg, Mn, Zn, and high turbidity. Samples from Pond 2 South and Pond 3 were brown to light-brown in color, while the sample from the Pond 1 inlet was colorless. TDS for all three samples ranged from 4800 to 6800 mg/L.

On 10/09/14, the Fe chemistry of the Pond 1 inlet and Pond 2 North were drastically different. The total iron content in Pond 2 North was over four times as high as Pond 1 inlet (2215 mg/L Fe, 530 mg/L Fe). The redox potentials from Pond 1 inlet and Pond 2 North were comparable to those from the 05/22/14 sampling. Pond 1

Table 1 SEM Inc. water quality data—sampled 05/22/14

Parameter	Units	Pond 1 (near the inlet)	Pond 2S	Pond 3
pH (lab)	pH	2.84	2.64	3.76
pH (field)	pH	2.65	2.59	3.72
Temperature (lab)	°C	18.5	19.3	18.7
Temperature (field)	°C	18.2	15.4	20.3
Redox potential	mV	663	721	621
Total dissolved solids	mg/L	5100	4800	6800
Turbidity	NTU	1.5	3.7	19
Alkalinity, Total	mg/L $CaCO_3$	<2	<2	<2
Alkalinity/bicarbonate	mg/L $CaCO_3$	<2	<2	<2
Alkalinity/carbonate	mg/L $CaCO_3$	<2	<2	<2
Alkalinity/hydroxide	mg/L $CaCO_3$	<2	<2	<2
Aluminum	mg/L	270	280	190
Antimony	mg/L	<0.002	<0.002	<0.002
Arsenic	mg/L	4.6	2.1	0.02
Barium	mg/L	0.006	0.002	0.008
Beryllium	mg/L	0.01	0.01	0.01
Boron	mg/L	0.11	0.1	0.31
Cadmium	mg/L	0.023	0.029	0.11
Calcium	mg/L	140	160	310
Chloride	mg/L	8	9	13
Chromium	mg/L	0.56	0.57	0.048
Cobalt	mg/L	1.4	1.4	4.2
Copper	mg/L	0.72	1.3	1.1
Ferric iron	mg/L	70	280	<1
Ferrous iron	mg/L	390	32	8
Fluoride	mg/L	6	6	10
Iron (total)	mg/L	460	310	7.4
Lead	mg/L	<0.002	<0.002	<0.002
Magnesium	mg/L	38	39	650
Manganese	mg/L	9.1	8.8	24
Mercury	mg/L	<0.0001	<0.0001	<0.0001
Nickel	mg/L	4	4.9	9.2
Nitrate	mg/L N	0.22	<0.05	1.2
Phosphorus (total)	mg/L	3.2	1.7	0.07
Potassium	mg/L	7.5	0.53	<0.5
Selenium	mg/L	<0.01	<0.01	<0.01
Silica	mg/L SiO_2	84	79	42
Silver	mg/L	<0.002	<0.002	<0.002
Sodium	mg/L	28	14	30
Sulfate	mg/L	3300	3200	4800
Thallium	mg/L	0.15	0.008	0.024
Zinc	mg/L	0.72	0.72	2.3

inlet had lower redox potential than Pond 2 North; 619 versus 794 mV, respectively. Once more, Pond 1 contained dominantly Fe^{2+}, while Pond 2 North contained almost entirely Fe^{3+}; Fe^{3+}/Fe^{2+} ratios for Pond 1 inlet and Pond 2 North were 0.060 and 146, respectively. Pond 2 North had an extremely high TDS of 33000 mg/L, while Pond 1 had a value comparable to the 05/22/14 sampling. The Pond 2 North sample was dark brown in color, while the sample from the Pond 1 inlet was again colorless.

Table 2 SEM Inc. water quality data—sampled 10/09/14

Parameter	Units	Pond 1 (at the inlet)	Pond 1 (North Shore)	Pond 2 N
Ferric iron	mg/L	30		2200
Ferrous iron	mg/L	500		15
Iron (total)	mg/L	530		2215
pH (lab)	pH	3.09		2.31
pH (field)	pH	2.97	2.78	2.23
Temperature (lab)	°C	21.2		21.2
Temperature (field)	°C	18.1	17.4	22.2
Redox potential	mV	619		794
Total dissolved solids	mg/L	3700		33000
Turbidity	NTU	11		2.4

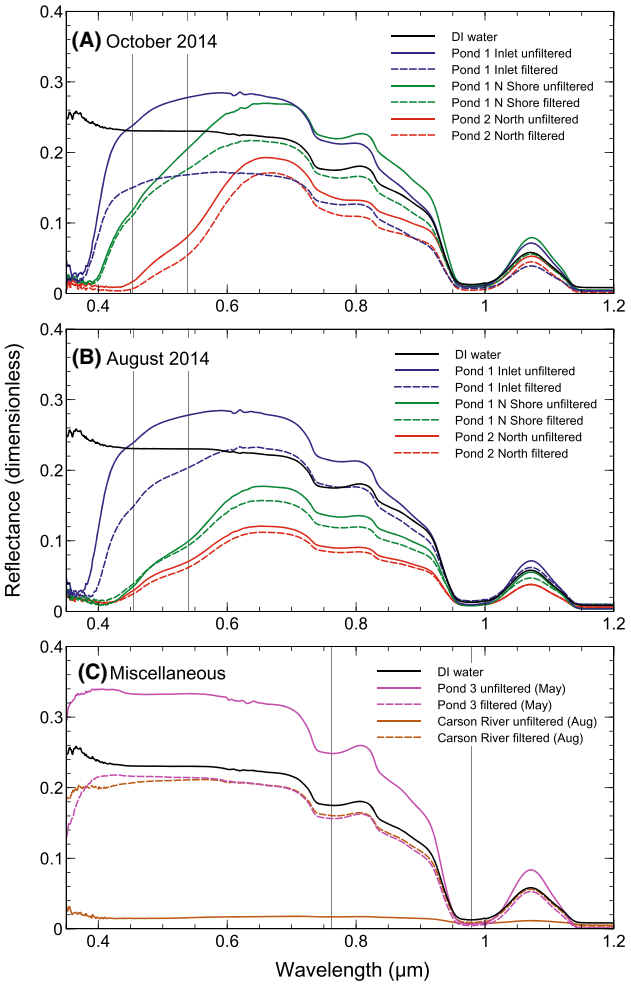

Fig. 3 Unfiltered samples are *solid lines* and filtered samples are *dashed lines*. *Gray bars* are placed at prominent absorption feature wavelengths. **a**, **b** 0.453, 0.54 μm; **c** 0.763, 0.975 μm

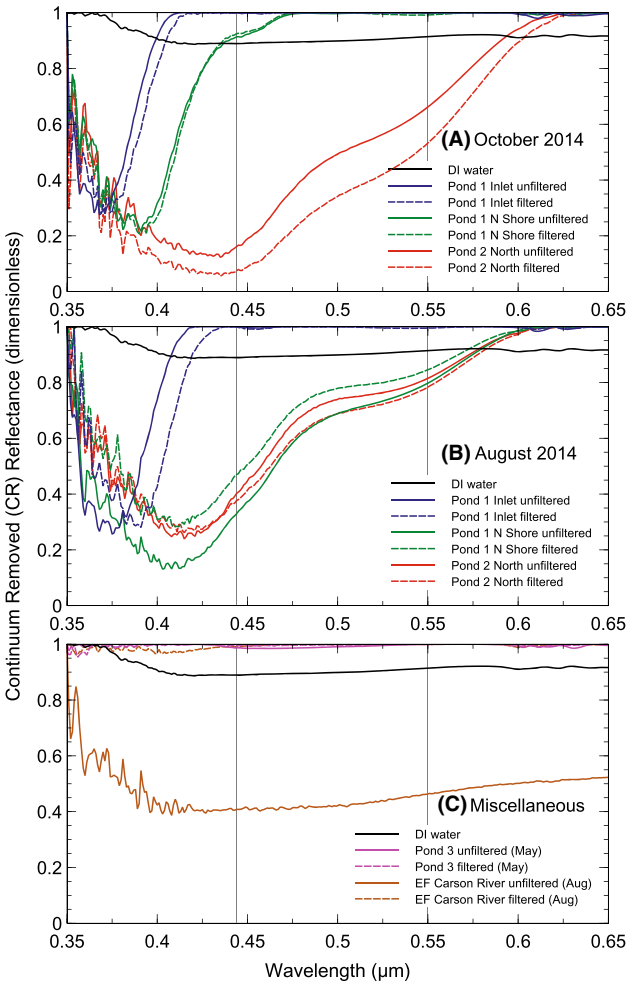

Fig. 4 Unfiltered samples are *solid lines* and filtered samples are *dashed lines*. *Gray bars* are placed at prominent absorption feature wavelengths (0.44, 0.55 μm)

Water Spectroscopy

All spectral curves for local AMD water are displayed in Figs. 3 and 4. The DI water spectral curve was relatively featureless until the appearance of broad absorption features centered at 0.763 and 0.975 μm, followed by a steep decreasing slope to virtually 100 % absorption beyond 1.15 μm (Fig. 3c). This spectral curve served as a "blank"

and demonstrated the spectral features of pure water. The absorption features at 0.763, 0. 975 μm, and beyond 1.15 μm were characteristic of the water molecule in the liquid phase (Dozier and Painter 2004; Green et al. 2006). Liquid water exhibits multiple absorption features between 0.4 and 2.5 μm, which result from combinations of three fundamental vibrational modes of the water molecule. These fundamental absorptions occur beyond the VSWIR region near 2.9, 3.1, and 6.1 μm, but their combinations and overtones occur in the VSWIR region (Green et al. 2006).

Generally, the curves of local AMD were characterized by virtually no reflectance below 0.4 μm, with an increasing slope through the blue/green regions (0.4–0.65 μm), and a peak reflectance between 0.65 and 0.66 μm (Fig. 3a, b). The absorption features in the local AMD curves were identical to those in the DI water curve from 0.763 μm onward. There was notable variation between local AMD waters in the 0.35–0.65 μm region. Pond 1 from the inlet had the least absorption in the blue/green region with a very slight inflection point at 0.453 μm. Pond 1 from the north shore had more absorption in the blue/green region with a more pronounced 0.453 μm inflection, and emergence of a second absorption feature at 0.54 μm. Pond 2 North had the lowest reflectance level in the blue/green region and a prominent 0.54 μm shoulder. Pond 3 had low reflectance on the edge of the UV, but did not exhibit any absorption features in the blue/green region (Fig. 3c). It had a curve more closely resembling that of DI water. The turbid Carson River sample was essentially featureless with no reflectance (Fig. 3c).

There was little variation in spectral features between the filtered and unfiltered local AMD. However, the filtered samples generally had lower overall reflectance than their unfiltered counterparts, with the exception being the filtered Carson River sample, which had a curve almost identical to that of DI water after filtering removed all suspended sediments.

In CR format, the region of greatest interest was between 0.35 and 0.625 μm (Fig. 4). An absorption feature occurred in the blue/green region for both Pond 1 and Pond 2 North (Fig. 4a, b). In August and October, Pond 1 from the inlet had an absorption feature centered at wavelengths <0.38 μm. Pond 1 from the north shore in October had an absorption feature centered at slightly longer wavelengths and a second smaller feature between 0.43 and 0.47 μm. Pond 2 North had the broadest overall absorption centered at the longest wavelengths with two features centered near 0.44 and 0.55 μm. In August, the Pond 1 north shore and Pond 2 North spectral shapes are quite similar to each other and most similar to the shape from Pond 2 North in October. Pond 3 and the filtered Carson River had no absorption features in this range (Fig. 4c). The unfiltered Carson River showed lower overall CR reflectance, however the spectral shape was dramatically different than the AMD curves.

Synthetic AMD Solutions

Water Spectroscopy

Spectral curves for synthetic AMD are displayed in Figs. 5 and 6. The Fe^{3+} solutions had virtually no reflectance below 0.4 μm, then steeply increased from 0.38 to 0.433 μm followed by an inflection point centered at 0.453 μm (Fig. 5a). Peak reflectance occurred at about 0.66 μm, followed by a broad absorption feature centered at 0.763 μm and a second feature centered at 0.975 μm, with near 100 % absorption beyond 1.15 μm. With

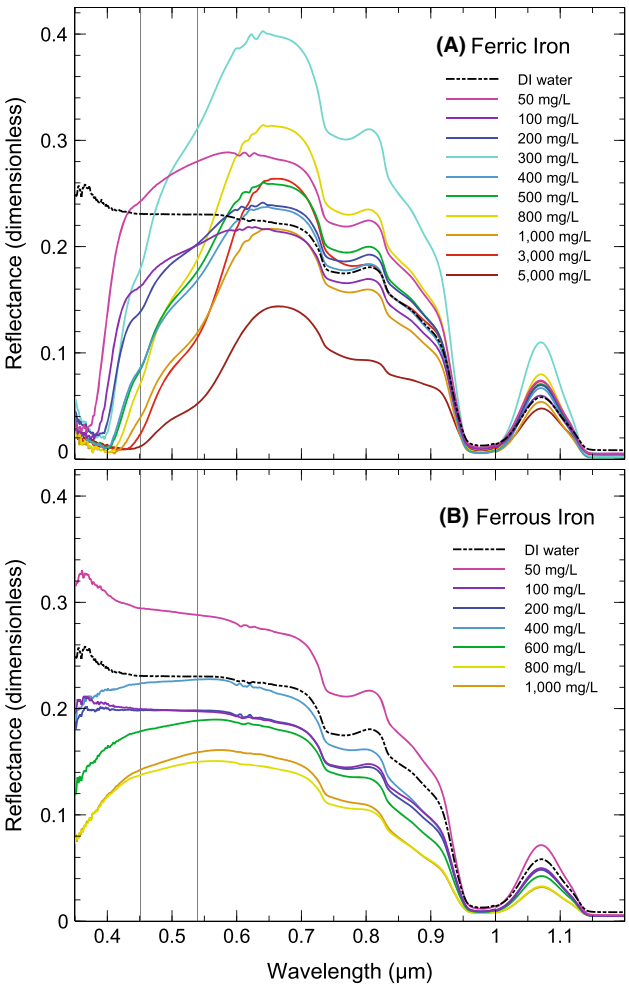

Fig. 5 Synthetic lab solutions demonstrating the spectral effect of **a** ferric and **b** ferrous iron in incrementing concentrations. *Gray bars* are placed at prominent absorption feature wavelengths (0.453, 0.54 μm). Addition of ferric and ferrous iron draw down reflectance in the *blue/green* region

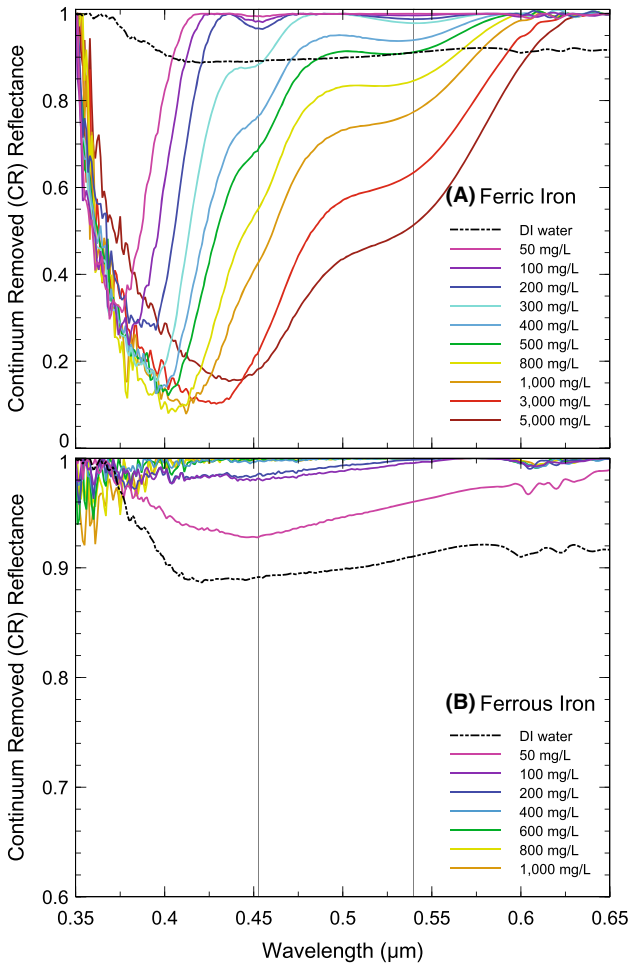

Fig. 6 Synthetic lab solutions demonstrating the spectral effect of **a** ferric and **b** ferrous iron in incrementing concentrations, in continuum removed mode. *Gray bars* are placed at prominent absorption feature wavelengths (0.453, 0.54 μm)

increasing Fe^{3+} concentration, the inflection point at 0.453 μm began to deepen. Approaching higher concentrations, a shoulder appeared at 0.54 μm, masking the shorter wavelength feature. Generally, reflectance decreased as ferric sulfate concentrations increased.

In CR format, the absorption feature occurring in the blue/green region broadened, and the band center shifted to longer wavelengths in the higher Fe^{3+} concentration solutions (Fig. 6a). For example, the 50 mg/L Fe^{3+} solution's band center occurred at 0.375 μm, while the 5000 mg/L ferric iron solution's band center was at 0.438 μm. Two absorption features also occurred at 0.453 and 0.54 μm. The 0.453 μm feature was most pronounced in concentrations below 500 mg/L Fe^{3+}. Above 500 mg/L Fe^{3+}, this feature became a small inflection in the expanded envelope of the blue/green absorption band.

The spectrum of the lower concentration Fe^{2+} solutions strongly resembled the spectrum for DI water (Fig. 5b). Absorption features in the 50 mg/L Fe^{2+} solution curves were identical to those in the DI water curve, and subsequent concentrations exhibited increasing absorption only at the shortest wavelengths. A small inflection point at 0.48 μm appeared in the 600 mg/L Fe^{2+} solution and deepened with increasing iron concentrations. In CR format, any absorption in the blue/green region was very minimal (Fig. 6b). At higher Fe^{2+} concentrations, although the absolute reflectance decreased in the blue-green, the CR process followed the contour of the original reflectance spectrum, so that there was no feature in the CR plot. At wavelengths 0.35–0.4 μm, the highest Fe^{2+} concentration solutions exhibited deeper band depths.

Discussion

Water Chemistry

The speciation of the aqueous iron has been illustrated in supplemental Fig. 3 based on the measured redox potential and pH of the local AMD. Aqueous iron occurs chiefly as sulfate complexes ($FeSO_4^+$, $FeSO_4^0$) and insoluble iron as Fe^{3+} oxyhydroxide (goethite, α-FeOOH). In natural waters, Fe^{3+} forms strong complexes with many ligands (Cl^-, SO_4^{2-}, $H_2PO_4^-$, F^-, HPO_4^{2-}, OH^-) (Langmuir 1997). Sulfate is by far the dominant anion present in the local AMD. The common solid products of AMD tend to be of small particle size, specifically ferrihydrite, schwertmannite, and goethite, which are characteristically in particles <10 nm in size (Murad and Rojik 2005). Thus, it is plausible for colloidal size goethite to flow through the 0.45 μm pores in the filter membranes. Gammons et al. (2009) noted that a common source of colorant in pit lake waters is the oxidation of dissolved iron to hydrous ferric oxide (HFO), a red-brown substance that is very fine-grained and slow to settle. HFOs include ferrihydrite, lepidocrocite, limonite, and goethite. It is therefore reasonable to assume the speciation of iron in Leviathan's AMD waters occurs primarily as ferric iron complexed with sulfate anions, or colloidal goethite (HFOs).

This speciation is consistent with the analytical data from Pond 2; however, the analytical data from the Pond 1 inlet shows that the iron is chiefly present as Fe^{2+}. The old tunnel in which the AMD emanates at Leviathan was reported to extend 135 meters below the surface (Evans 1977). At that depth, the redox potential may be lower than at the surface discharge elevation, which would be consistent with the speciation of aqueous iron as Fe^{2+}. Throughout its journey from groundwater to surface water discharge, the AMD is slowly oxidizing as it reaches equilibrium with the atmosphere, so that water at the south

end of Pond 1 (by the inlet pipe) is more reduced than the water on the north end of the Pond 1 and in Pond 2.

Spectroscopy

Local AMD Waters

Nearly all of the filtered samples have lower total reflectance than their unfiltered equivalents (Fig. 3). This is consistent with the Tyndall effect, which is the effect of light scattering by particles in a colloid or particles in a fine suspension (Brown et al. 2006). The filtered samples have lower total reflectance because there are fewer particles in suspension that will scatter light and increase reflectance leaving the water. The exception to this was the unfiltered Carson River sample, which was turbid enough to reverse the Tyndall effect through suspended sediments absorbing virtually all of the incoming light from the ASD's halogen probe.

There is very little difference in the spectral absorption features of filtered and unfiltered samples when analyzed in reflectance and CR formats. This suggests that most of the coloring agent in local AMD is an ion or a colloidal fraction <0.45 μm in size. It should be noted that the local AMD has relatively low turbidity (1.5–11 NTU). It is not surprising that the spectral responses of these waters are not predominately caused by larger suspended particles.

Synthetic AMD Solutions

In this study, all ferric iron influenced waters are characterized by a rapid decrease in reflectance at shorter wavelengths. Additional absorption bands centered at 0.453 and 0.54 μm occur. As noted in the previous section, the most likely cause of color is Fe^{3+} complexed with sulfates, or colloidal HFOs such as ferrihydrite, lepidocrocite, limonite, and goethite. Absorption spectra of ferric oxide and sulfate minerals have been presented by a number of previous studies (e.g. Cloutis et al. 2006; Crowley et al. 2003, 2006; Sherman and Waite 1985). Ferric iron in minerals has a number of electronic absorption features related to charge transfer between the ferric cation and associated oxygen anions; the strong absorption edge may also be due to magnetic coupling of ferric ions (Sherman and Waite 1985). In minerals, the crystallography will impart mineral specific absorption features due to the distortion of the electronic configuration of the iron cation by the crystal structure and surrounding atoms. For iron complexed with sulfates or hydrous oxides in solution, crystal field transitions are not expected, but the absorption features of the synthetic AMD are similar to that seen in ferric oxides and sulfates, and are attributed to ligand field and ligand–metal charge transfer transitions. These absorption bands occur near 0.360–0.80, 0.430, and 0.485–0.550 μm (Sherman and Waite 1985), which is consistent with the 0.453 and 0.54 μm absorption bands identified in the study's water spectra.

The CR spectra show a consistent correlation between Fe^{3+} concentration in solution and VSWIR diagnostic features. The depth and extent of the absorption features in the region between 0.35 and 0.625 μm may provide a reliable approximation of Fe^{3+} concentration in aqueous solutions (Fig. 6a). To quantify the depth of the absorption band due to Fe^{3+}, the integrals of the CR curves were calculated for synthetic AMD solutions in the wavelength range 0.35–0.625 μm. When the integral values were plotted against the iron concentrations, a calibration curve with an r-squared value of 0.96 was produced (Fig. 7). The Fe^{3+} concentration (x) may be estimated using the equation $x = e^{(y + 0.38)/0.1063}$, where y equals the integrated band depth between 0.35 and 0.625 μm.

Ferrous iron impacts the spectral reflectance by absorbing wavelengths below 0.6 μm, but CR reflectance does not quantify ferrous iron's contribution effectively. At wavelengths 0.35–0.4 μm, the band depth of absorption generally correlates with Fe^{2+} concentrations (Fig. 6b). However, this is an extremely noisy region in the ASD spectrometer's range and is challenging to examine in detail. The depth of this absorption band is also extremely shallow compared to the band depths caused by Fe^{3+} (Fig. 6a, b). Additionally, it may be very difficult to confidently identify spectral absorption features specifically owing to Fe^{2+} in environmental samples when Fe^{3+} exhibits more robust features in the same wavelength region.

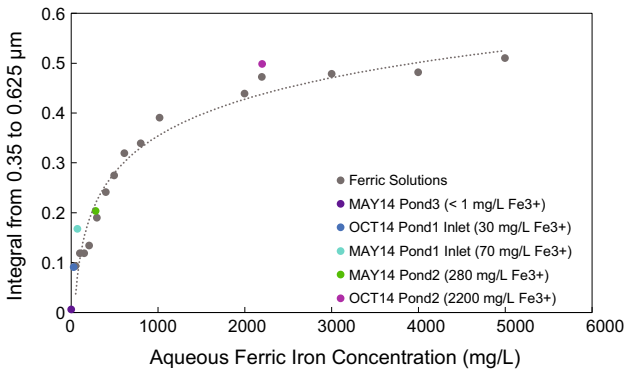

Fig. 7 Plot of Fe^{3+} concentration versus $\int_{0.350}^{0.625} CR\ Reflectance\ dx$. AMD sample points (*colored*) are filtered and have known Fe^{3+} concentration from SEM Inc. analysis. Synthetic AMD solutions (*gray*) from laboratory experiment. *Trend line* equation $y = 0.1063\ln(x) - 0.38$ and $R^2 = 0.9618$. The *calibration curve* is pH dependent (pH range 3.1–7)

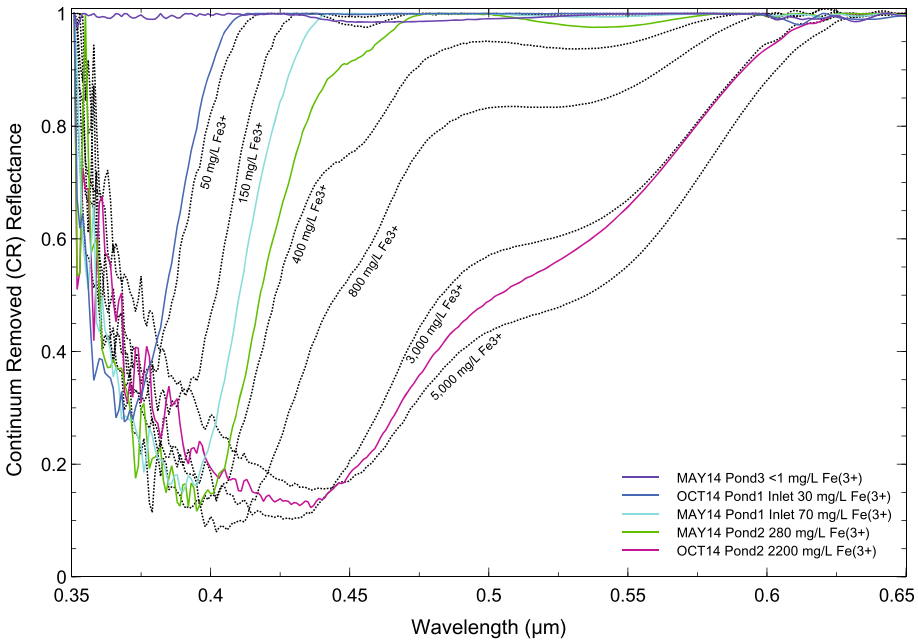

Fig. 8 Colored plots are local AMD samples with known Fe concentration (from SEM Inc. analysis). Local AMD samples are unfiltered. Dotted contour plots are from synthetic AMD solutions

Correlation of Local and Synthetic Waters

All local AMD water CR curves plot agreeably within the range established by the synthetic AMD solution CR curves (Fig. 8). Over the course of this study, the Fe^{3+} concentration at the Pond 1 inlet fluctuated between 30 and 70 mg/L Fe^{3+}, whereas the concentration of Pond 2 fluctuated between 280 and 2200 mg/L Fe^{3+}. Pond 1 represents freshly discharged AMD, while Pond 2 represents a more evapo-concentrated AMD. This variation is distinguishable in the VSWIR spectral response of local AMD water. The Fe^{3+} concentration can be approximated using the synthetic AMD curves as contour lines (Fig. 8). The Pond 1 inlet curves consistently plot closer to the 50–300 mg/L Fe^{3+} contour lines, while the Pond 2 curves plot closer to high concentration contour lines.

This method appears to be most accurate for lower Fe^{3+} concentrations. The local AMD waters with concentrations <500 mg/L Fe^{3+} plot closer to their respective synthetic AMD contour lines. The local AMD sample with over 2000 mg/L Fe^{3+} has the most error, i.e. greatly overestimating iron concentration.

There is a problematic dynamic when measuring iron by VSWIR reflectance if most of the iron is in the reduced form. Ferrous iron lacks diagnostic VSWIR features that are easily measured using basic spectral reflectance analysis techniques. The methods described in this paper may be limited to only highly oxidized AMD.

Mine waters are highly variable in their composition and may be dominated by numerous dissolved constituents and thermodynamic conditions depending on the geologic environment in which they originate (Lottermoser 2003). The methods described in this paper may not be suitable for all AMD. Similar to optical studies of natural water bodies, the inherent and apparent optical properties of AMD are influenced by a range of physical, biological, and chemical processes, which may interfere with accurate estimation of constituents based on spectral signatures. We recommend that this method for aqueous ferric iron concentration estimation be restricted to mine waters that are acidic (pH range 2–6) due to the oxidation of iron rich sulfides, commonly found at base metal, gold, and coal mines. Highly turbid waters should be filtered or allowed to settle before employing this method. If the water volume is too turbid for light to effectively penetrate the column, the resulting spectrum should not be examined for Fe^{3+} concentration.

Conclusion

The spectral response of Fe^{3+}-dominated AMD in the VSWIR region is unique. Compared with non-iron rich impaired water, turbid river water, and DI water, the AMD from Leviathan Mine possessed distinct characteristics that may be used for diagnostic identification. Specifically, the region between 0.35 and 0.625 μm may be used to approximately quantify Fe^{3+} concentration. This method may be best suited for mine waters that are acidic, high in sulfate, and low in turbidity. Ferric iron concentration is a useful value that may imply other parameters such as pH, Eh, and general water quality. Subtle changes in Fe^{3+}

concentration due to environmental and seasonal conditions at Leviathan Mine were identified using VSWIR spectroscopy alone. These findings suggest subtle changes in mine water quality may also be identified qualitatively and quantitatively via remote spectroscopy.

Acknowledgments We thank Doug Carey and Taylor Zetner from the Lahontan Regional Water Quality Control Board for granting us access to the Leviathan Mine Superfund site. Acknowledgement is extended to Dr. Simon Poulson and Dr. Glenn Miller for serving as advisory committee members, and graduate student Neil Pearson for additional support. Funding for this project was provided by the National Aeronautics and Space Administration (NASA) HyspIRI Preparatory Airborne Activities for Energy and Mineral Resources through Grant NNX12AQ17G to the University of Nevada, Reno.

References

Brown TL, LeMay HE, Bursten BE, Murphy CJ (2006) Chemistry: the central science. Ch 13, properties of solutions, 10th edn. Prentice-Hall, Upper Saddle River

Burns RG (1993) Origin of electronic spectra of minerals in the visible to near-infrared region. Remote geochemical analysis: elemental and mineralogic composition. Cambridge University Press, New York, pp 3–29

California Regional Water Quality Control Board, Lahontan Region (2015) Year-end report for the 2014 field season at Leviathan Mine. http://www.swrcb.ca.gov/lahontan/water_issues/projects/leviathan_project/docs/lev2014rpt.pdf. Accessed 20 Aug 2015

Castendyk DN, Eary LE (2009) Mine pit lakes—characteristics, predictive modeling, and sustainability. Ch 1, the nature and global distribution of Pit Lakes, vol 3, Soc for Mining, Metallurgy, and Exploration (SME), electronic edn, pp 1–11

Clark RN, Roush TL (1984) Reflectance spectroscopy: quantitative analysis techniques for remote sensing applications. J Geophys Res 89(B7):6329–6340. doi:10.1029/JB089iB07p06329

Cloutis EA, Hawthorne FC, Mertzman SA, Krenn K, Craig MA, Marcino D, Methot M, Strong J, Mustard JF, Blaney DL, Bell JF, Vilas F (2006) Detection and discrimination of sulfate minerals using reflectance spectroscopy. Icarus 184(1):121–157. doi:10.1016/j.icarus.2006.04.003

Crowley JK, Williams DE, Hammarstrom JM, Piatak N, Chou IM, Mars JC (2003) Spectral reflectance properties (0.4–2.5 μm) of secondary Fe-oxide, Fe-hydroxide, and Fe-sulphate-hydrate minerals associated with sulphide-bearing mine wastes. Geochem Explor Environ Anal 3(3):219–228. doi:10.1144/1467-7873/03-001

Crowley JK, Williams DE, Hammarstrom JM, Piatak N, Mars JC, Chou IM (2006) Spectral reflectance properties (0.4–2.5 um) of secondary Fe-oxide, Fe-hydroxide, and Fe-sulfate-hydrate minerals associated with sulfide-bearing mine waste. US Geological Survey OFR 2003-196, Washington, DC

Dozier J, Painter TH (2004) Multispectral and hyperspectral remote sensing of alpine snow properties. Ann Rev Earth Planet Sci 32:465–494. doi:10.1146/annurev.earth.32.101802.120404

Duaime TE, Tucci NJ (2009) Butte mine flooding operable unit water-level monitoring and water-quality sampling, 2008 consent decree update. Montana Bureau of Mines and Geology Open File Report 589

Evans JR (1977) Zaca mine and Leviathan mine. In: Mines and mineral resources of alpine county, California, county report 8. California Div of Mines and Geology, pp 22–27

Gammons CH, Harris LN, Castro LM, Cott PA, Hanna BW (2009) Creating lakes from open pit mines: process and considerations, with emphasis on northern environments. Can Tech Rep Fish Aquat Sci 2826:1–106

Green RO, Painter TH, Roberts DA, Dozier J (2006) Measuring the expressed abundance of the three phases of water with an imaging spectrometer over melting snow. Water Resour Res 42(W10402):1–12. doi:10.1029/2005wr004509

Hunt GR, Ashley RP (1979) Spectra of altered rocks in the visible and near infrared. Econ Geol 74:1613–1629. doi:10.2113/gsecongeo.74.7.1613

Kruse FA, Lefkoff AB, Dietz JB (1993) Expert system-based mineral mapping in northern Death Valley, California/Nevada, using the Airborne Visible/Infrared Imaging Spectrometer (AVIRIS). Remote Sens Environ 44:309–336. doi:10.1016/0034-4257(93)90024-R

Langmuir D (1997) Aqueous environmental geochemistry. Ch12: iron and sulfur geochemistry. Prentice-Hall, Upper Saddle River, pp 431–474

Lottermoser BG (2003) Mine wastes. Ch 3: mine water. Springer, New York City, pp 83–141

McCullough CD, Müller M, Eulitz K, Lund MA (2011) Modelling a pit lake district to plan for abstraction regime changes. In: Proc, Mine Closure Conf, Alberta, Canada, pp 581–592

Murad E, Rojik P (2005) Iron mineralogy of mine-drainage precipitates as environmental indicators: review of current concepts and a case study from the Sokolov Basin, Czech Republic. Clay Miner 40:427–440. doi:10.1180/0009855054040181

Peichang S, Cheng S, Smith S (2004) Acid lake identification using GIS and remote sensing. In: Proceedings of Geological Soc of America, annual meeting, vol 36(5), p 300

Sanliyuksel D, Yucel MA, Baba A (2014) Change detection and visualization of acid mine lakes using time series satellite image data in geographic information systems (GIS): Can (Canakkale) County, NW Turkey. Environ Earth Sci 72:4311–4323. doi:10.1007/s12665-014-3330-6

Sherman DM, Waite TD (1985) Electronic spectra of Fe^{3+} oxides and oxide hydroxides in the near IR to near UV. Am Mineral 70:1262–1269

Shevenell LA (2000) Water quality in pit lakes in disseminated gold deposits compared to two natural, terminal lakes in Nevada. Environ Geol 36(7):807–815. doi:10.1007/s002540050497

Vandersluis GD, Straskraba V, Effner SA (1995) Hydrogeological and geochemical aspects of lakes forming in abandoned open pit mines. Proc, water resources at risk. https://www.imwa.info/docs/imwa_1995/IMWA1995_Vandersluis.pdf